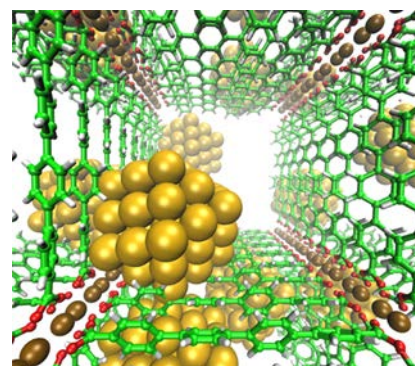


Encapsulation of Au₅₅ Clusters within Surface-Supported Metal–Organic Frameworks for Catalytic Reduction of 4-Nitrophenol

Jinxuan Liu, Shahriar Heidrich, Jianxi Liu, Biao Guo, Michael Zharnikov, Ulrich Simon,
**||*

ABSTRACT: We demonstrate a facile approach to encapsulate ligand stabilized Au₅₅ clusters [Au₅₅(PPh₃)₁₂Cl₆] within highly oriented surface supported metal–organic framework (SURMOF) thin films via liquid phase epitaxy. The Au₅₅ clusters were successfully loaded into the pores of SURMOF during their fabrication, which has been confirmed by X ray diffraction, infrared spectroscopy, and ultraviolet–visible spectroscopy. Computational modeling reveals that there is a strong interaction between the Au₅₅ core and the oligophenyl ligands of the MOF pore, leading to a removal of the PPH₃ ligands. The stabilized Au₅₅ clusters within SURMOF exhibit excellent catalytic activity for the reduction of 4 nitrophenol.



KEYWORDS: SURMOF, Au cluster, liquid phase epitaxy, catalysis, conductivity

INTRODUCTION

In the past decade, metal–organic frameworks (MOFs) have been one of the most intensively investigated classes of materials. This huge interest results from the tunable chemical and physical properties of these materials, which are fabricated by the interconnection of organic linkers via metal or metal/oxo clusters.^{1,2} In addition, it has been demonstrated in many cases that the performance of MOFs in a variety of application fields can be substantially enhanced by loading the guest species into the pores of these molecular frameworks.^{3–7} Numerous approaches have been established to load objects of appropriate size, such as metal nanoparticles (NPs),^{8–10} quantum dots,^{11,12} and biomolecules,^{13–16} into the voids of these porous, crystalline materials. Of particular interest is the loading with metallic NPs, which can render additional functionality to the molecular frameworks, for example, in the context of catalysis^{5,17,18} and optical properties.^{19,20} As regards the former, Au nanoclusters show significantly enhanced activity and selectivity in chemical reactions when supported on oxides.²¹

Previous strategies to load metal NPs into MOFs include chemical vapor deposition using volatile organometallic precursors,^{22,23} solution infiltration using metal ions,^{24–28} solid grinding using organometallic compounds,^{29,30} and pressure induced amorphization.³¹ In several cases, a two step strategy was applied, where first the guest species were loaded into the pores using one of the methods described above. Then, in a second step, these guests were modified

further by chemical treatments. Particularly attractive in this connection is to first load with metal oxide NPs, which are then reduced with H₂ by either heating or microwave treatments.³²

On the other hand, the as synthesized metal NPs can be directly integrated into the cavities during the MOF fabrication via surface functionalization^{19,33–40} or physical vapor deposition.⁴¹

With regard to a number of applications, integration of these framework compounds into the devices is required. When it comes to more advanced functionalities, often the powder form of MOFs, as obtained by conventional MOF synthesis schemes, is not well suited. In particular, if good electrical conductivity, good thermal contact to a substrate, or good optical properties are required, it is of significant advantage to fabricate MOFs in the form of thin films. With regard to device integration, surface supported MOFs (SURMOFs) fabricated using layer by layer (lbl) deposition procedures have received increasing attention, and related applications as membranes, catalysts, sensors, and photovoltaic devices have been reported.^{42,43}

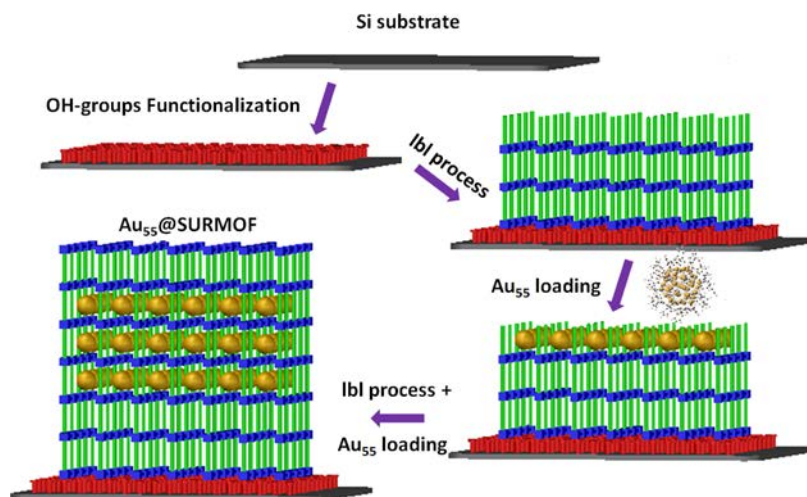


Figure 1. Schematic illustration of the fabrication process for the idealized sandwich like structure of Au_{55} @SURMOF.

Successful lbl deposition of SURMOFs has been reported for a variety of different substrates. An interesting feature of this fabrication strategy is that the loading with large guest species can be combined with the lbl construction of SURMOFs, that is, the loading of moieties which are smaller than a MOF pore but larger than the channels connecting the pores becomes possible as schematically shown in Figure 1.⁴⁴

Herein, we demonstrate a facile strategy for the encapsulation of Au_{55} clusters during the lbl construction of SURMOFs. Specifically, we used the $\text{Au}_{55}(\text{PPh}_3)_{12}\text{Cl}_6$ clusters, also known as “Schmid cluster”,⁴⁵ with a core diameter of 1.4 nm and a diameter of 2 nm including the ligand shell. These clusters, which were stabilized by suitable ligands, were highly monodisperse and had a well defined composition. They were subsequently loaded into two different MOF types of the SURMOF 2 family, Cu QPDC and Cu PPDC CH_3 .⁴⁶ Successful loading was then confirmed by X ray diffraction (XRD) where a pronounced change in form factor revealed that virtually every pore had been filled with Au NPs (we use NPs instead of “clusters” here and below). Computational reconstruction of the crystal structure from XRD data suggests an unexpected interaction of the Au_{55} NPs with the linkers forming the pore walls, leading to a removal of some of the triphenylphosphine ligands and a “cornering” of these NPs, while density functional theory (DFT) calculations^{47,48} agree with the experimental finding of substantially increased conductivity upon loading.

EXPERIMENTAL SECTION

Preparation of $\text{Au}_{55}(\text{PPh}_3)_{12}\text{Cl}_6$ NPs. The structure of the $\text{Au}_{55}(\text{PPh}_3)_{12}\text{Cl}_6$ NPs is shown in Figure 2. The Au_{55} NPs used in this study were synthesized according to a previously reported procedure.⁴⁹ Ultraviolet–visible (UV–vis) spectra of $\text{Au}_{55}(\text{PPh}_3)_{12}\text{Cl}_6$ recorded for dichloromethane suspensions are shown in Figure S1.

SURMOFs can be grown on a variety of differently functionalized substrates using a variety of different MOF types. For an overview, see recent review articles.⁴² In this study, we focus on MOF thin films of the type SURMOF 2 using (Cu^{2+}) dimers as connectors and QPDC (quarterphenyl dicarboxylate) and PPDC (pentaphenyl dicarboxylate) as organic linkers.⁴⁶

Preparation of Cu-QPDC and Cu-PPDC- CH_3 SURMOFs. Empty reference SURMOFs were grown on modified Si substrates using the lbl procedure (Figure 1). XRD data recorded for these reference samples are shown in Figure S2; they are fully consistent with the results reported previously.⁴⁶

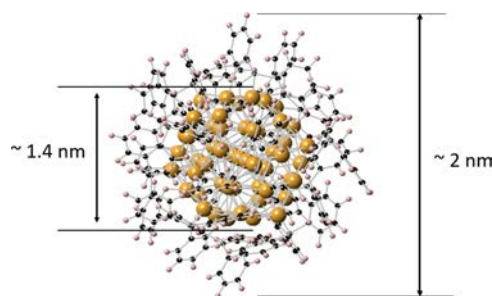


Figure 2. Schematic representation of $\text{Au}_{55}(\text{PPh}_3)_{12}\text{Cl}_6$ NP.

Preparation of $\text{Au}_{55}(\text{PPh}_3)_{12}\text{Cl}_6$ @Cu-QPDC and $\text{Au}_{55}(\text{PPh}_3)_{12}\text{Cl}_6$ @Cu-PPDC- CH_3 SURMOFs. The $\text{Au}_{55}(\text{PPh}_3)_{12}\text{Cl}_6$ @Cu QPDC and $\text{Au}_{55}(\text{PPh}_3)_{12}\text{Cl}_6$ @Cu PPDC CH_3 SURMOFs were prepared using a modified lbl construction scheme of SURMOFs with a homemade spray setup.⁵⁰

The procedure is illustrated in Figure 1.

First, the Si substrate was functionalized with hydroxyl groups by exposing it to oxygen plasma for about 15 min. After that, the functionalized substrate was mounted on a sample holder, and an empty Cu QPDC or Cu PPDC CH_3 SURMOF was prepared by alternatively spraying a 1 mM ethanolic solution of $\text{Cu}_2(\text{CH}_3\text{COO})_4 \cdot \text{H}_2\text{O}$ and a 20 mM ethanolic solution of QPDC or PPDC CH_3 at room temperature. The fabrication of Au NP loaded SURMOF 2 structures was then carried out by adding an additional step to the lbl deposition sequence. More precisely, after each assembly step [$\text{Cu}_2(\text{CH}_3\text{COO})_4 \cdot \text{H}_2\text{O}$, QPDC, or PPDC CH_3] a solution containing $\text{Au}_{55}(\text{PPh}_3)_{12}\text{Cl}_6$ NPs was sprayed onto the empty Cu QPDC or Cu PPDC CH_3 template, followed by a subsequent spraying of the solution of $\text{Cu}_2(\text{CH}_3\text{COO})_4 \cdot \text{H}_2\text{O}$, QPDC, or PPDC CH_3 (see Figure 1). By repetition of this process $\text{Au}_{55}(\text{PPh}_3)_{12}\text{Cl}_6$ @Cu QPDC and $\text{Au}_{55}(\text{PPh}_3)_{12}\text{Cl}_6$ @Cu PPDC CH_3 SURMOFs were prepared. In the last assembly step, additional empty Cu QPDC and Cu PPDC CH_3 layers were constructed. Finally, a sandwich like $\text{Au}_{55}(\text{PPh}_3)_{12}\text{Cl}_6$ @Cu QPDC and $\text{Au}_{55}(\text{PPh}_3)_{12}\text{Cl}_6$ @Cu PPDC CH_3 SURMOFs were obtained (Figure 1). It should be noted that the solution of $\text{Au}_{55}(\text{PPh}_3)_{12}\text{Cl}_6$ NPs was sprayed only after spraying of QPDC or PPDC CH_3 solution.

The as prepared samples were further characterized by using XRD, infrared reflection–absorption (IRRA) spectroscopy, and UV–vis spectroscopy.

Characterization of $\text{Au}_{55}(\text{PPh}_3)_{12}\text{Cl}_6$ @Cu-QPDC and $\text{Au}_{55}(\text{PPh}_3)_{12}\text{Cl}_6$ @Cu-PPDC- CH_3 SURMOFs. Out of plane and in plane XRD measurements were carried out using two different diffractometers, a Bruker D8 Advance and a Bruker D8 Discover, both

equipped with Cu anodes utilizing the Cu $K\alpha_{1,2}$ radiation ($\lambda = 0.15419$ nm). The out of plane XRD data were acquired over the 2θ range of $2-20^\circ$, with 168 s per 0.024° step. The in plane XRD data were recorded over the 2θ range of $2-20^\circ$, with 100 s per 0.024° step. The IRRA spectra of the $\text{Au}_{55}(\text{PPh}_3)_{12}\text{Cl}_6@$ Cu PPDC CH_3 SURMOF were recorded with a resolution of 2 cm^{-1} using a Bruker VERTEX 80 spectrometer under ambient conditions. An incident angle of 80° and a liquid nitrogen cooled narrow band mercury cadmium telluride detector were used. The UV-vis spectra were recorded on a high performance Agilent Cary 5000 UV-vis-NIR spectrophotometer.

Electrical Conductivity Measurement Using a Mercury-Drop-Based Tunneling Junction. The Cu QPDC and $\text{Au}_{55}@$ Cu QPDC SURMOFs were integrated in a tunneling junction for electric transport property characterization. A mercury drop setup was used.⁵¹ Briefly, we first used a gastight Hamilton syringe to extrude the mercury drop, which was then passivated with hexadecanethiol (HDT) to avoid amalgamation and short circuit. The passivated mercury drop was gently made to come in contact with the SURMOF electrode to build the mercury drop based tunneling junction (Hg/HDT//SURMOF/Au) in a cell filled with HDT in hexadecane. A camera was used to monitor the contact of mercury drop to the SURMOF and measure the contact area.

Catalytic Reduction of 4-Nitrophenol. The catalytic performance of $\text{Au}_{55}(\text{PPh}_3)_{12}\text{Cl}_6@$ Cu QPDC SURMOF for the reduction of 4 nitrophenol was tested in a 3 mL quartz cuvette using an UV-vis spectrometer (Agilent 8453 instrument). Aqueous 4 nitrophenol solution (0.1 mM) was added to 1.5 mL of tetrahydrofuran in a cuvette. Subsequently, the $\text{Au}_{55}(\text{PPh}_3)_{12}\text{Cl}_6@$ Cu QPDC SURMOF was immersed into the above mixture, followed by 1 mL of freshly prepared NaBH_4 solution (0.02 M). The cuvette was then placed in the sample holder of the UV-vis spectrometer without stirring the solution, and the consecutive UV-vis absorption spectra were recorded over the suitable time frame.

Computational Modeling. (001)/(002) XRD peak intensity ratios were obtained for the atomistic structures by calculating the intensities according to

$$I = \sum_i \left(2 \sum_{j<i} f_i f_j \cdot \cos(2\pi \mathbf{G}_{hkl} \cdot \mathbf{R}_{ij}) + f_i^2 \right) \cdot \text{LP}(\theta(\mathbf{G}_{hkl}))$$

where i and j are atom indices, f_i and f_j are the atomic form factors, \mathbf{G}_{hkl} is the reciprocal lattice vector corresponding to the peak, \mathbf{R}_{ij} is the distance vector between the atoms i and j , and $\text{LP}(\theta)$ is the Lorentz polarization correction given by

$$\text{LP}(\theta) = \frac{1 + \cos^2(2\theta)}{2 \sin^2(\theta) \cos(\theta)}$$

The intensity ratios were calculated for "cutouts" consisting of $9 \times 9 \times 9$ Cu QPDC unit cells, with one Au_{55} cluster in each $3 \times 1 \times 1$ cell. Au_{55} cluster positions and orientations were varied systematically until a (001)/(002) intensity ratio close to the experiment (cf. Figure 4) was obtained for the case of uniformly orientated clusters displaced at random toward one of the four pore corners by around 7 Å from the pore center.

We also performed ab initio calculations using DFT to estimate the effect of loading with $\text{Au}_{55}(\text{PPh}_3)_{12}\text{Cl}_6$ on charge carrier mobilities along the SURMOF channels. To this end, the unloaded MOF was represented as a "network" of bond saturated QPDC linkers (Figure S3a), while the MOF loading was modeled by placing the "naked", channel centered Au_{55} clusters in every third unit cell (Figure S3b). Hopping rates k_{CT} in the channel direction for these two models were then calculated according to the Marcus theory⁵²

$$k_{\text{CT}} = \frac{2\pi}{\hbar} |V_{\text{if}}|^2 \sqrt{\frac{1}{4\pi k_B T \lambda}} \exp\left(-\frac{(\lambda + \Delta E_{\text{if}})^2}{4\lambda k_B T}\right)$$

where V_{if} are electronic couplings, λ are reorganization energies, $T = 300$ K is the temperature, and ΔE_{if} is the energy difference between

the initial and final states, which was set to zero here as we neglect energetic disorder. Reorganization energies were calculated for linkers and clusters in vacuum according to the Nelson's four point procedure.⁵³ Electronic couplings were estimated using the direct coupling scheme⁵⁴ considering only the highest occupied and lowest unoccupied molecular orbitals (HOMO and LUMO, respectively) as follows

$$V_{\text{if}} = \frac{\langle \phi_A | F | \phi_B \rangle - 1/2(\langle \phi_A | F | \phi_A \rangle + \langle \phi_B | F | \phi_B \rangle) \langle \phi_A | S | \phi_B \rangle}{1 - \langle \phi_A | S | \phi_B \rangle^2}$$

where ϕ_A and ϕ_B are the LUMO (HOMO) of the electron (hole) donor and acceptor molecules, respectively. For Au_{55} , HOMO and LUMO were replaced by the singly occupied molecular orbital's two spin channels. F is the Fock operator for the dimer system and S denotes taking the overlap.

Mobilities were estimated from the rates according to⁵⁵

$$\mu = \frac{eL^2}{k_B T} k_{\text{CT}}$$

where L is the distance between the relevant molecules or clusters. Specific values for the two systems and intermediate results can be found in Table S1.

All DFT calculations were carried out using the B3LYP exchange-correlation functional and def2 SVP basis set as implemented in the TURBOMOLE package.⁵⁶

RESULTS AND DISCUSSION

We first focus on the Cu QPDC SURMOF 2, which exhibits a pore size of 2.2 nm. Figure 3a displays the experimental XRD patterns of the empty and the Au NP loaded SURMOFs normalized to the intensity of the (002) diffraction peak. Comparison of the XRD data of the loaded SURMOF with the empty one reveals that the relative intensity of the (001) peak

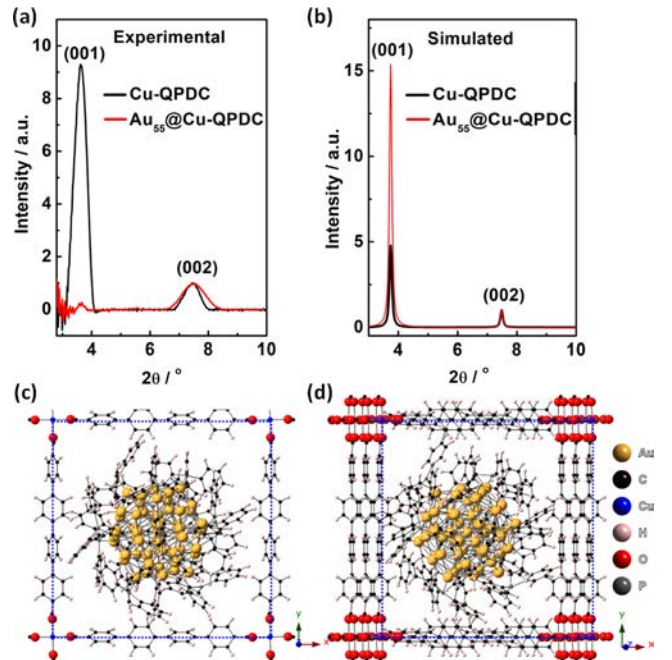


Figure 3. Out of plane experimental (a) and simulated (b) XRD data of Cu QPDC and $\text{Au}_{55}(\text{PPh}_3)_{12}\text{Cl}_6@$ Cu QPDC SURMOF along the (001) direction. The experimental and simulated intensities are normalized to the (002) peak. Front (c) and side (d) views of the unit cell of fully loaded $\text{Au}_{55}(\text{PPh}_3)_{12}\text{Cl}_6@$ Cu QPDC (3×1 loading, see text). Note the poor agreement of the XRD simulations with the experimental data.

is substantially decreased upon loading with the Au NPs. This change in XRD form factor directly demonstrates a successful loading of the Au NPs into the MOF cavities.⁵⁷

To quantitatively analyze the loading amount of Au NPs into Cu QPDC SURMOF 2, in situ quartz crystal microbalance (QCM) measurements were carried out. The observed frequency drop (Figure S4) indicates the successful loading of $\text{Au}_{55}(\text{PPh}_3)_{12}\text{Cl}_6$ into Cu QPDC SURMOF 2, while the quantitative analysis of the QCM data gives a $\text{Au}_{55}(\text{PPh}_3)_{12}\text{Cl}_6$ loading of 170 ng, which corresponds to a loading fraction of roughly 25%. Within the error bars, this value is consistent with the 3×1 unit cell shown in Figure S5.

In order to facilitate the analysis of the XRD data, simulations of the XRD patterns were carried out using fully loaded $\text{Au}_{55}(\text{PPh}_3)_{12}\text{Cl}_6@$ Cu QPDC (100%) SURMOF structures, as shown in Figure 3c,d. The corresponding simulated XRD patterns of the $\text{Au}_{55}(\text{PPh}_3)_{12}\text{Cl}_6@$ Cu QPDC SURMOFs are displayed in Figure 3b. The relative intensity of the (001) peak of $\text{Au}_{55}(\text{PPh}_3)_{12}\text{Cl}_6@$ Cu QPDC SURMOFs (100%) strongly increased with increased Au particle loading, in obvious disagreement with the experimental XRD results (in Figure 3a).

In order to better understand the reason for this unexpected disagreement between the experiment and simulation, we applied a search strategy where a “naked” Au_{55} cluster (assuming the positions of the Au atoms are the same as in the $\text{Au}_{55}(\text{PPh}_3)_{12}\text{Cl}_6$ cluster) was placed inside the pore and then allowed to move freely. A systematic search for (001)/(002) peak intensity ratios matching the experiment (see the Supporting Information) leads to the structure depicted in Figure 4a. While for such a “cornered” structure a reasonable

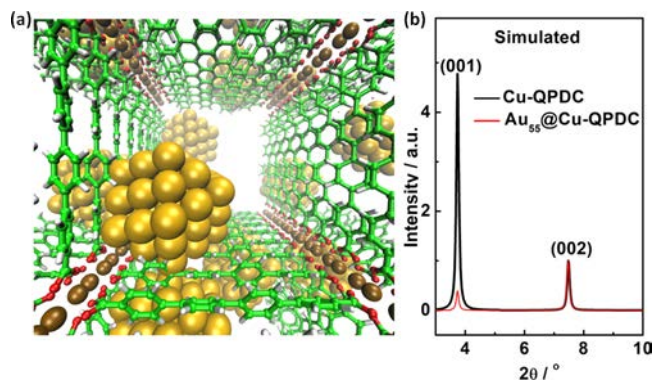


Figure 4. (a) Proposed location of “naked” Au_{55} clusters in the pores of the Cu QPDC SURMOF 2. According to the theoretical results, the ligand stripped clusters are best stabilized in the highly coordinated corners of the cell of Cu QPDC SURMOF 2. Such positions are not accessible with the PPh_3 ligands in place (see Figure 3). (b) Simulated XRD pattern of $\text{Au}_{55}@$ Cu QPDC SURMOF along the (001) direction. Note that the agreement of the simulations with the experimental data (in particular the intensity of the (001) diffraction peak) shown in Figure 3a is substantially improved.

agreement between the experimental and simulated XRD patterns is observed (Figure 4b), this structure is not consistent with the presence of the PPh_3 ligands at the surface of the Au NP. It is however known that these ligands, which are necessary to stabilize Au_{55} in solution, can easily get stripped from the core of the particle if a competitive binding site that can stabilize the core is present.^{58,59} Relying on these literature results, we thus propose that upon interaction of the

$\text{Au}_{55}(\text{PPh}_3)_{12}\text{Cl}_6$ clusters with the oligophenyl backbone of the MOF linkers the PPh_3 ligands are at least partially displaced to yield direct Au_{55} –phenyl interactions, as indicated in Figure 4a. Note that the calculation of the XRD pattern in Figure 4b was carried out for Au_{55} , while removal of the PPh_3 ligands yields $\text{Au}_{55}\text{Cl}_6$. The effect of adding six Cl atoms on the XRD pattern and on the precise location of the Au cluster within the MOF pore was considered to be negligible.

To further demonstrate the successful loading of $\text{Au}_{55}(\text{PPh}_3)_{12}\text{Cl}_6$ within Cu QPDC SURMOF, the conductivity of empty Cu QPDC and $\text{Au}_{55}(\text{PPh}_3)_{12}\text{Cl}_6@$ Cu QPDC SURMOFs was measured in a mercury drop based tunneling junction.⁵¹ The current flowing through the Hg/HDT//SURMOF/Au junction was measured by sweeping the bias voltage in the negative (−1.5 to −0.01 V) and positive range (+0.01 to +1.5 V). Figure S6 shows the semilog plot of the current density J under the applied voltage V for the Cu QPDC (black line) and $\text{Au}_{55}(\text{PPh}_3)_{12}\text{Cl}_6@$ Cu QPDC (blue line). We found that the conductivity of $\text{Au}_{55}(\text{PPh}_3)_{12}\text{Cl}_6@$ Cu QPDC SURMOFs was by ~ 4 orders of magnitude higher than that of the empty Cu QPDC. Such a significant effect indicates the successful loading of $\text{Au}_{55}(\text{PPh}_3)_{12}\text{Cl}_6$ into Cu QPDC. This is in qualitative agreement with the results of our DFT calculations, according to which charge carrier mobilities for hopping between the Au_{55} clusters are around 1 order of magnitude higher than those for hopping between the MOF linkers in channel direction (Table S1). The remaining discrepancy between predicted and experimental values can be attributed to the loading induced effects not considered here, such as changing of the injection barrier or facilitation of second order hopping processes.⁶⁰

It has been reported that the ligand stabilized atomically precise gold nanoclusters (Au_{23} , Au_{24} , Au_{25}) can be used as a catalyst for the reduction of 4 nitrophenol.^{61–63} In this context, we utilized $\text{Au}_{55}(\text{PPh}_3)_{12}\text{Cl}_6@$ Cu QPDC SURMOF as a catalyst for 4 nitrophenol reduction to 4 aminophenol. Figure 5 shows the time evolution of the UV–vis absorption spectra

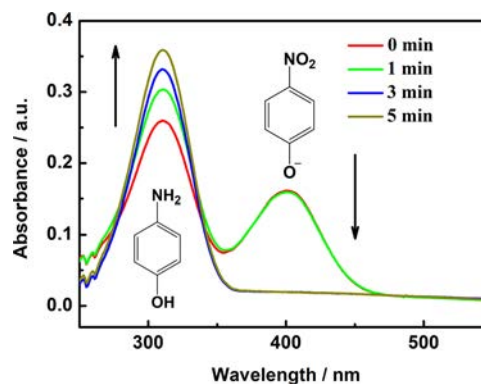


Figure 5. Consecutive UV–vis absorption spectra measured in the course of the catalytic reduction of 4 nitrophenol over the $\text{Au}_{55}(\text{PPh}_3)_{12}\text{Cl}_6@$ Cu QPDC SURMOF.


in the course of such a catalytic reaction. Accordingly, 4 nitrophenol was completely reduced to 4 aminophenol within 5 min compared to the pure $\text{Au}_{55}(\text{PPh}_3)_{12}\text{Cl}_6$ within 10 min (Figure S7). Thus, the $\text{Au}_{55}(\text{PPh}_3)_{12}\text{Cl}_6@$ Cu QPDC SURMOF exhibits superior catalytic properties in the 4 NP reduction reaction, which stems presumably from the detailed atomic packing modes and electronic structure.

CONCLUSIONS

Using an lbl process, the ligand stabilized Au₅₅ nanoclusters could be loaded into the pores of a SURMOF thin film reaching loading factors of around 25%. A thorough analysis of the XRD data suggests that the Au nanoclusters attach to the phenyl rings present at the corners of the SURMOF pores. As a result, at least some of the triphenylphosphine ligands stabilizing the pristine Au₅₅ are removed. The Au₅₅ clusters integrated within the SURMOFs lead to a substantial increase of electrical conductivity and exhibit excellent catalytic activity for the reduction of 4 nitrophenol.


AUTHOR INFORMATION


Corresponding Author

Christof Wöll – Institute of Functional Interfaces, Karlsruhe Institute of Technology, 76344 Eggenstein Leopoldshafen, Germany;  orcid.org/0000 0003 1078 3304; Email: christof.woell@kit.edu

Authors


Jinxuan Liu – State Key Laboratory of Fine Chemicals, School of Chemical Engineering, Dalian University of Technology, 116024 Dalian, China;  orcid.org/0000 0002 6306 1359

Shahriar Heidrich – Institute of Nanotechnology, Institute of Functional Interfaces, Karlsruhe Institute of Technology, 76344 Eggenstein Leopoldshafen, Germany;  orcid.org/0000 0002 9691 4012

Jianxi Liu – State Key Laboratory of Solidification Processing, Center of Advanced Lubrication and Seal Materials, Northwestern Polytechnical University, Xi'an 710072, Shaanxi, China;  orcid.org/0000 0002 6394 600X

Biao Guo – State Key Laboratory of Fine Chemicals, School of Chemical Engineering, Dalian University of Technology, 116024 Dalian, China

Michael Zharnikov – Applied Physical Chemistry/Institute for Physical Chemistry, Heidelberg University, 69120 Heidelberg, Germany

Ulrich Simon – Institute of Inorganic Chemistry, RWTH Aachen University, 52056 Aachen, Germany;  orcid.org/0000 0002 6118 0573

Wolfgang Wenzel – Institute of Nanotechnology, Institute of Functional Interfaces, Karlsruhe Institute of Technology, 76344 Eggenstein Leopoldshafen, Germany

Author Contributions

The manuscript was written through contributions of all authors. All authors have given approval to the final version of the manuscript.

Notes

The authors declare no competing financial interest.

ACKNOWLEDGMENTS

Financial support from the National Natural Science Foundation of China (NSFC 21673032), the Fundamental Research Funds for the Central Universities of China (DUT18RC(3)055), the China Postdoctoral Science Foundation (2020T130532), the State Key Laboratory of Physical Chemistry of Solid Surfaces, Xiamen University (201812), and the Deutsche Forschungsgemeinschaft (DFG, German Research Foundation) under Germany's Excellence Strategy—2082/1—390761711 is gratefully acknowledged. We thank Dr. Tobias Wächter for assistance during the electrical conductivity measurements and Dr. Tobias Schlöder for fruitful discussions.

REFERENCES

- (1) Yaghi, O. M. Reticular Chemistry Construction, Properties, and Precision Reactions of Frameworks. *J. Am. Chem. Soc.* **2016**, *138*, 15507–15509.
- (2) Kitagawa, S.; Kitaura, R.; Noro, S. i. Functional porous coordination polymers. *Angew. Chem., Int. Ed.* **2004**, *43*, 2334–2375.
- (3) Aijaz, A.; Xu, Q. Catalysis with Metal Nanoparticles Immobilized within the Pores of Metal Organic Frameworks. *J. Phys. Chem. Lett.* **2014**, *5*, 1400–1411.
- (4) Cheon, Y. E.; Suh, M. P. Enhanced Hydrogen Storage by Palladium Nanoparticles Fabricated in a Redox Active Metal Organic Framework. *Angew. Chem., Int. Ed.* **2009**, *48*, 2899–2903.
- (5) Cirujano, F. G.; Luz, I.; Soukri, M.; Van Goethem, C.; Vankelecom, I. F. J.; Lail, M.; De Vos, D. E. Boosting the Catalytic Performance of Metal Organic Frameworks for Steroid Transformations by Confinement within a Mesoporous Scaffold. *Angew. Chem., Int. Ed.* **2017**, *56*, 13302–13306.
- (6) Yang, Q.; Liu, W. X.; Wang, B. Q.; Zhang, W. N.; Zeng, X. Q.; Zhang, C.; Qin, Y. J.; Sun, X. M.; Wu, T. P.; Liu, J. F.; Huo, F. W.; Lu, J. Regulating the spatial distribution of metal nanoparticles within metal organic frameworks to enhance catalytic efficiency. *Nat. Commun.* **2017**, *8*, 14429.
- (7) Ye, Y.; Guo, W.; Wang, L.; Li, Z.; Song, Z.; Chen, J.; Zhang, Z.; Xiang, S.; Chen, B. Straightforward Loading of Imidazole Molecules into Metal Organic Framework for High Proton Conduction. *J. Am. Chem. Soc.* **2017**, *139*, 15604–15607.
- (8) Dhakshinamoorthy, A.; Garcia, H. Catalysis by metal nanoparticles embedded on metal organic frameworks. *Chem. Soc. Rev.* **2012**, *41*, 5262–5284.
- (9) Meilikhov, M.; Yusenko, K.; Esken, D.; Turner, S.; Van Tendeloo, G.; Fischer, R. A. Metals@MOFs Loading MOFs with Metal Nanoparticles for Hybrid Functions. *Eur. J. Inorg. Chem.* **2010**, *2010*, 3701–3714.
- (10) Moon, H. R.; Lim, D. W.; Suh, M. P. Fabrication of metal nanoparticles in metal organic frameworks. *Chem. Soc. Rev.* **2013**, *42*, 1807–1824.
- (11) Esken, D.; Noei, H.; Wang, Y.; Wiktor, C.; Turner, S.; Van Tendeloo, G.; Fischer, R. A. ZnO@ZIF 8: stabilization of quantum confined ZnO nanoparticles by a zinc methylimidazolate framework and their surface structural characterization probed by CO₂ adsorption. *J. Mater. Chem.* **2011**, *21*, 5907–5915.
- (12) Esken, D.; Turner, S.; Wiktor, C.; Kalidindi, S. B.; Van Tendeloo, G.; Fischer, R. A. GaN@ZIF 8: Selective Formation of Gallium Nitride Quantum Dots inside a Zinc Methylimidazolate Framework. *J. Am. Chem. Soc.* **2011**, *133*, 16370–16373.

- (13) Feng, D. W.; Liu, T. F.; Su, J.; Bosch, M.; Wei, Z. W.; Wan, W.; Yuan, D. Q.; Chen, Y. P.; Wang, X.; Wang, K. C.; Lian, X. Z.; Gu, Z. Y.; Park, J.; Zou, X. D.; Zhou, H. C. Stable metal organic frameworks containing single molecule traps for enzyme encapsulation. *Nat. Commun.* **2015**, *6*, 5979.
- (14) Rother, M.; Nussbaumer, M. G.; Renggli, K.; Bruns, N. Protein cages and synthetic polymers: a fruitful symbiosis for drug delivery applications, bionanotechnology and materials science. *Chem. Soc. Rev.* **2016**, *45*, 6213–6249.
- (15) Shieh, F. K.; Wang, S. C.; Yen, C. I.; Wu, C. C.; Dutta, S.; Chou, L. Y.; Morabito, J. V.; Hu, P.; Hsu, M. H.; Wu, K. C. W.; Tsung, C. K. Imparting Functionality to Biocatalysts via Embedding Enzymes into Nanoporous Materials by a de Novo Approach: Size Selective Sheltering of Catalase in Metal Organic Framework Microcrystals. *J. Am. Chem. Soc.* **2015**, *137*, 4276–4279.
- (16) Zeng, J. Y.; Zhang, M. K.; Peng, M. Y.; Gong, D.; Zhang, X. Z. Porphyrinic Metal Organic Frameworks Coated Gold Nanorods as a Versatile Nanoplatfor for Combined Photodynamic/Photothermal/Chemotherapy of Tumor. *Adv. Funct. Mater.* **2018**, *28*, 1705451–1705463.
- (17) Guo, J.; Zhang, X.; Sun, Y.; Tang, L.; Liu, Q.; Zhang, X. Loading Pt Nanoparticles on Metal Organic Frameworks for Improved Oxygen Evolution. *ACS Sustain. Chem. Eng.* **2017**, *5*, 11577–11583.
- (18) Yu, J.; Mu, C.; Yan, B.; Qin, X.; Shen, C.; Xue, H.; Pang, H. Nanoparticle/MOF composites: preparations and applications. *Mater. Horiz.* **2017**, *4*, 557–569.
- (19) Lu, G.; Li, S.; Guo, Z.; Farha, O. K.; Hauser, B. G.; Qi, X.; Wang, Y.; Wang, X.; Han, S.; Liu, X.; DuChene, J. S.; Zhang, H.; Zhang, Q.; Chen, X.; Ma, J.; Loo, S. C. J.; Wei, W. D.; Yang, Y.; Hupp, J. T.; Huo, F. Imparting functionality to a metal organic framework material by controlled nanoparticle encapsulation. *Nat. Chem.* **2012**, *4*, 310–316.
- (20) Song, T.; Yu, J.; Cui, Y.; Yang, Y.; Qian, G. Encapsulation of dyes in metal organic frameworks and their tunable nonlinear optical properties. *Dalton Trans.* **2016**, *45*, 4218–4223.
- (21) Pei, Y.; Shao, N.; Gao, Y.; Zeng, X. C. Investigating Active Site of Gold Nanoparticle Au55(PPh3)12Cl6 in Selective Oxidation. *ACS Nano* **2010**, *4*, 2009–2020.
- (22) Hermes, S.; Schröter, M. K.; Schmid, R.; Khodeir, L.; Muhler, M.; Tissler, A.; Fischer, R. W.; Fischer, R. A. Metal@MOF: Loading of highly porous coordination polymers host lattices by metal organic chemical vapor deposition. *Angew. Chem., Int. Ed.* **2005**, *44*, 6237–6241.
- (23) Schröder, F.; Esken, D.; Cokoja, M.; van den Berg, M. W.; Lebedev, O. I.; van Tendeloo, G.; Walaszek, B.; Buntkowsky, G.; Limbach, H. H.; Chaudret, B.; Fischer, R. A. Ruthenium nanoparticles inside porous [Zn4O(bdc)3] by hydrogenolysis of adsorbed [Ru(cod)(cot)]: a solid state reference system for surfactant stabilized ruthenium colloids. *J. Am. Chem. Soc.* **2008**, *130*, 6119–6130.
- (24) Aijaz, A.; Karkamkar, A.; Choi, Y. J.; Tsumori, N.; Rönnebro, E.; Autrey, T.; Shioyama, H.; Xu, Q. Immobilizing Highly Catalytically Active Pt Nanoparticles inside the Pores of Metal Organic Framework: A Double Solvents Approach. *J. Am. Chem. Soc.* **2012**, *134*, 13926–13929.
- (25) Gu, X.; Lu, Z. H.; Jiang, H. L.; Akita, T.; Xu, Q. Synergistic Catalysis of Metal Organic Framework Immobilized Au Pd Nano particles in Dehydrogenation of Formic Acid for Chemical Hydrogen Storage. *J. Am. Chem. Soc.* **2011**, *133*, 11822–11825.
- (26) Houk, R. J. T.; Jacobs, B. W.; Gabaly, F. E.; Chang, N. N.; Talin, A. A.; Graham, D. D.; House, S. D.; Robertson, I. M.; Allendorf, M. D. Silver Cluster Formation, Dynamics, and Chemistry in Metal–Organic Frameworks. *Nano Lett.* **2009**, *9*, 3413–3418.
- (27) Park, T. H.; Hickman, A. J.; Koh, K.; Martin, S.; Wong Foy, A. G.; Sanford, M. S.; Matzger, A. J. Highly Dispersed Palladium(II) in a Defective Metal Organic Framework: Application to C H Activation and Functionalization. *J. Am. Chem. Soc.* **2011**, *133*, 20138–20141.
- (28) Zlotea, C.; Campesi, R.; Cuevas, F.; Leroy, E.; Dibandjo, P.; Volkringer, C.; Loiseau, T.; Ferey, G.; Latroche, M. Pd Nanoparticles Embedded into a Metal Organic Framework: Synthesis, Structural Characteristics, and Hydrogen Sorption Properties. *J. Am. Chem. Soc.* **2010**, *132*, 2991–2997.
- (29) Jiang, H. L.; Liu, B.; Akita, T.; Haruta, M.; Sakurai, H.; Xu, Q. Au@ZIF 8: CO Oxidation over Gold Nanoparticles Deposited to Metal–Organic Framework. *J. Am. Chem. Soc.* **2009**, *131*, 11302–11303.
- (30) Jiang, H. L.; Lin, Q. P.; Akita, T.; Liu, B.; Ohashi, H.; Oji, H.; Honma, T.; Takei, T.; Haruta, M.; Xu, Q. Ultrafine Gold Clusters Incorporated into a Metal Organic Framework. *Chem.—Eur. J.* **2011**, *17*, 78–81.
- (31) Chapman, K. W.; Sava, D. F.; Halder, G. J.; Chupas, P. J.; Nenoff, T. M. Trapping Guests within a Nanoporous Metal Organic Framework through Pressure Induced Amorphization. *J. Am. Chem. Soc.* **2011**, *133*, 18583–18585.
- (32) El Shall, M. S.; Abdelsayed, V.; Khder, A. E. R. S.; Hassan, H. M. A.; El Kaderi, H. M.; Reich, T. E. Metallic and bimetallic nanocatalysts incorporated into highly porous coordination polymer MIL 101. *J. Mater. Chem.* **2009**, *19*, 7625–7631.
- (33) Tsuruoka, T.; Kawasaki, H.; Nawafune, H.; Akamatsu, K. Controlled Self Assembly of Metal Organic Frameworks on Metal Nanoparticles for Efficient Synthesis of Hybrid Nanostructures. *ACS Appl. Mater. Interfaces* **2011**, *3*, 3788–3791.
- (34) Buso, D.; Jasieniak, J.; Lay, M. D. H.; Schiavuta, P.; Scopece, P.; Laird, J.; Amenitsch, H.; Hill, A. J.; Falcaro, P. Highly Luminescent Metal Organic Frameworks Through Quantum Dot Doping. *Small* **2012**, *8*, 80–88.
- (35) Sugikawa, K.; Nagata, S.; Furukawa, Y.; Kokado, K.; Sada, K. Stable and Functional Gold Nanorod Composites with a Metal Organic Framework Crystalline Shell. *Chem. Mater.* **2013**, *25*, 2565–2570.
- (36) Zhang, W.; Lu, G.; Li, S.; Liu, Y.; Xu, H.; Cui, C.; Yan, W.; Yang, Y.; Huo, F. Controlled incorporation of nanoparticles in metal organic framework hybrid thin films. *Chem. Commun.* **2014**, *50*, 4296–4298.
- (37) Zhao, M.; Deng, K.; He, L.; Liu, Y.; Li, G.; Zhao, H.; Tang, Z. Core Shell Palladium Nanoparticle@Metal Organic Frameworks as Multifunctional Catalysts for Cascade Reactions. *J. Am. Chem. Soc.* **2014**, *136*, 1738–1741.
- (38) Ke, F.; Wang, L.; Zhu, J. An efficient room temperature core shell AgPd@MOF catalyst for hydrogen production from formic acid. *Nanoscale* **2015**, *7*, 8321–8325.
- (39) Shi, L.; Wang, T.; Zhang, H.; Chang, K.; Ye, J. Electrostatic Self Assembly of Nanosized Carbon Nitride Nanosheet onto a Zirconium Metal Organic Framework for Enhanced Photocatalytic CO2Reduction. *Adv. Funct. Mater.* **2015**, *25*, 5360–5367.
- (40) Wang, Z.; Gui, M.; Asif, M.; Yu, Y.; Dong, S.; Wang, H.; Wang, W.; Wang, F.; Xiao, F.; Liu, H. A facile modular approach to the 2D oriented assembly MOF electrode for non enzymatic sweat biosensors. *Nanoscale* **2018**, *10*, 6629–6638.
- (41) Yoshimaru, S.; Sadakiyo, M.; Staykov, A.; Kato, K.; Yamauchi, M. Modulation of the catalytic activity of Pt nanoparticles through charge transfer interactions with metal organic frameworks. *Chem. Commun.* **2017**, *53*, 6720–6723.
- (42) Liu, J.; Wöll, C. Surface supported metal organic framework thin films: fabrication methods, applications, and challenges. *Chem. Soc. Rev.* **2017**, *46*, 5730–5770.
- (43) Shekhah, O.; Liu, J.; Fischer, R. A.; Wöll, C. MOF thin films: existing and future applications. *Chem. Soc. Rev.* **2011**, *40*, 1081–1106.
- (44) Gu, Z. G.; Li, D. J.; Zheng, C.; Kang, Y.; Wöll, C.; Zhang, J. MOF Templated Synthesis of Ultrasmall Photoluminescent Carbon Nanodot Arrays for Optical Applications. *Angew. Chem., Int. Ed.* **2017**, *56*, 6853–6858.
- (45) Schmid, G. The relevance of shape and size of Au55 clusters. *Chem. Soc. Rev.* **2008**, *37*, 1909–1930.
- (46) Liu, J.; Lukose, B.; Shekhah, O.; Arslan, H. K.; Weidler, P.; Gliemann, H.; Brase, S.; Grosjean, S.; Godt, A.; Feng, X. L.; Mullen, K.; Magdau, I. B.; Heine, T.; Wöll, C. A novel series of isoreticular

metal organic frameworks: realizing metastable structures by liquid phase epitaxy. *Sci. Rep.* **2012**, *2*, 921.

(47) Vilhelmsen, L. B.; Walton, K. S.; Sholl, D. S. Structure and Mobility of Metal Clusters in MOFs: Au, Pd, and AuPd Clusters in MOF 74. *J. Am. Chem. Soc.* **2012**, *134*, 12807–12816.

(48) Yakovenko, A. A.; Wei, Z.; Wriedt, M.; Li, J. R.; Halder, G. J.; Zhou, H. C. Study of Guest Molecules in Metal Organic Frameworks by Powder X ray Diffraction: Analysis of Difference Envelope Density. *Cryst. Growth Des.* **2014**, *14*, 5397–5407.

(49) Schmid, G. Hexachlorododecakis(Tripphenyl phosphine) pentapentacontagold, Au₅₅[P(C₆H₅)₃]₁₂Cl₆. *Inorg. Synth.* **1990**, *7*, 214–218.

(50) Arslan, H. K.; Shekhah, O.; Wohlgemuth, J.; Franzreb, M.; Fischer, R. A.; Wöll, C. High Throughput Fabrication of Uniform and Homogenous MOF Coatings. *Adv. Funct. Mater.* **2011**, *21*, 4228–4231.

(51) Liu, J.; Wächter, T.; Irmeler, A.; Weidler, P. G.; Gliemann, H.; Pauly, F.; Mugnaini, V.; Zharnikov, M.; Wöll, C. Electric Transport Properties of Surface Anchored Metal Organic Frameworks and the Effect of Ferrocene Loading. *Acs Appl Mater Inter* **2015**, *7*, 9824–9830.

(52) Marcus, R. A. Electron transfer reactions in chemistry. Theory and experiment. *Rev. Mod. Phys.* **1993**, *65*, 599–610.

(53) Nelsen, S. F.; Blackstock, S. C.; Kim, Y. Estimation of inner shell Marcus terms for amino nitrogen compounds by molecular orbital calculations. *J. Am. Chem. Soc.* **1987**, *109*, 677–682.

(54) Stehr, V.; Pfister, J.; Fink, R. F.; Engels, B.; Deibel, C. First principles calculations of anisotropic charge carrier mobilities in organic semiconductor crystals. *Phys. Rev. B* **2011**, *83*, 155208–155221.

(55) Kera, S.; Yamane, H.; Ueno, N. First principles measurements of charge mobility in organic semiconductors: Valence hole vibration coupling in organic ultrathin films. *Prog. Surf. Sci.* **2009**, *84*, 135–154.

(56) Ahlrichs, R.; Bär, M.; Häser, M.; Horn, H.; Kölmel, C. Electronic structure calculations on workstation computers: The program system turbomole. *Chem. Phys. Lett.* **1989**, *162*, 165–169.

(57) Guo, W.; Liu, J.; Weidler, P. G.; Liu, J.; Neumann, T.; Danilov, D.; Wenzel, W.; Feldmann, C.; Wöll, C. Loading of ionic compounds into metal organic frameworks: a joint theoretical and experimental study for the case of La³⁺. *Phys. Chem. Chem. Phys.* **2014**, *16*, 17918–17923.

(58) Leifert, A.; Pan, Y.; Kinkeldey, A.; Schiefer, F.; Setzler, J.; Scheel, O.; Lichtenbeld, H.; Schmid, G.; Wenzel, W.; Jahnen Dechent, W.; Simon, U. Differential hERG ion channel activity of ultrasmall gold nanoparticles. *Proc. Natl. Acad. Sci. U.S.A.* **2013**, *110*, 8004–8009.

(59) Broda, J.; Setzler, J.; Leifert, A.; Steitz, J.; Benz, R.; Simon, U.; Wenzel, W. Ligand lipid and ligand core affinity control the interaction of gold nanoparticles with artificial lipid bilayers and cell membranes. *Nanomed. Nanotechnol.* **2016**, *12*, 1409–1419.

(60) Neumann, T.; Liu, J.; Wächter, T.; Friederich, P.; Symalla, F.; Welle, A.; Mugnaini, V.; Meded, V.; Zharnikov, M.; Wöll, C.; Wenzel, W. Superexchange Charge Transport in Loaded Metal Organic Frameworks. *ACS Nano* **2016**, *10*, 7085–7093.

(61) Shivhare, A.; Ambrose, S. J.; Zhang, H.; Purves, R. W.; Scott, R. W. J. Stable and recyclable Au₂₅clusters for the reduction of 4 nitrophenol. *Chem. Commun.* **2013**, *49*, 276–278.

(62) Zhao, S.; Das, A.; Zhang, H.; Jin, R.; Song, Y.; Jin, R. Mechanistic insights from atomically precise gold nanocluster catalyzed reduction of 4 nitrophenol. *Prog. Nat. Sci. Mater.* **2016**, *26*, 483–486.

(63) Yamamoto, H.; Yano, H.; Kouchi, H.; Obora, Y.; Arakawa, R.; Kawasaki, H. N,N Dimethylformamide stabilized gold nanoclusters as a catalyst for the reduction of 4 nitrophenol. *Nanoscale* **2012**, *4*, 4148–4154.

Repository KITopen

Dies ist ein Postprint/begutachtetes Manuskript.

Empfohlene Zitierung:

Liu, J.; Heidrich, S.; Liu, J.; Guo, B.; Zharnikov, M.; Simon, U.; Wenzel, W.; Wöll, C.
[Encapsulation of Au₅₅ Clusters within Surface-Supported Metal-Organic Frameworks for Catalytic Reduction of 4-Nitrophenol](#)
2020. ACS applied nano materials
[doi:10.5445/IR/1000129123](https://doi.org/10.5445/IR/1000129123)

Zitierung der Originalveröffentlichung:

Liu, J.; Heidrich, S.; Liu, J.; Guo, B.; Zharnikov, M.; Simon, U.; Wenzel, W.; Wöll, C.
[Encapsulation of Au₅₅ Clusters within Surface-Supported Metal-Organic Frameworks for Catalytic Reduction of 4-Nitrophenol](#)
2020. ACS applied nano materials, 4 (1), 522–528.
[doi:10.1021/acsanm.0c02842](https://doi.org/10.1021/acsanm.0c02842)

Lizenzinformationen: [KITopen-Lizenz](#)